Biointerface Research in Applied Chemistry
Open-Access Journal (ISSN: 2069-5837)

Article
Volume 16, Issue 1, 2026, 34
https://doi.org/10.33263/BRIAC161.034

Unveiling the Antitumor Potential of *Eugenia calycina* Fruit: *In silico* Exploration of NUDT Enzyme and Estrogen Receptor Alpha Inhibition

Fernanda Chairunisa [1], Tiyara Fany Mansyah [2], Dzikri Anfasa Firdaus [3,4], Maheswari Alfira Dwicesaria [2], Gusnia Meilin Gholam [2], Ayu Tri Nursyarah [2,4], Syahidatul Helma [4], Riyan Alifbi Putera Irsal [4,5,*]

1 Universitas Nasional, Department of Biology, South Jakarta, Indonesia; fernandachairunisa@civitas.unas.ac.id;
2 Bogor Agricultural University, Department of Biochemistry, Faculty of Mathematics and Natural Sciences, Bogor, Indonesia; gusniameilin@apps.ipb.ac.id;
3 Sultan Ageng Tirtayasa University, Department of Food Technology, Faculty of Agriculture, Serang, Indonesia; dzikri.anfasa@untirta.ac.id;
4 Biomatics, Bogor, West Java, Indonesia; bioinforid23@gmail.com;
5 Kyushu University, Department of Applied Chemistry, Faculty of Engineering, Fukuoka, Japan; irsal.riyan.342@s.kyushu-u.ac.jp;
* Correspondence: irsal.riyan.342@s.kyushu-u.ac.jp;

Received: 9.07.2025; Accepted: 15.11.2025; Published: 15.02.2026

Abstract: Estrogen receptor alpha (ERα) and NUDT5 overexpression are hallmarks of aggressive breast cancer, associated with poor prognosis and therapeutic resistance. This study investigates *Eugenia calycina*, a plant rich in bioactive compounds, for its potential as an anti-breast cancer agent. We focus on its effects on ERα and NUDT5, an enzyme involved in cancer progression. This study combines molecular docking, DFT, and MD simulations to evaluate *Eugenia calycina*'s phytochemicals for targeting ERα and NUDT5. The results indicate that PDB2 exhibits superior binding stability compared to reference compounds, as evidenced by lower $RMSD_{backbone}$ and RMSF values in molecular dynamics simulations. Furthermore, MM-PBSA calculations revealed significantly more negative binding free energies for PDB2 with both NUDT5 and ERα, suggesting stronger interactions. Quantum chemical calculations provided insights into the electronic properties of the compounds, revealing PDB2's potential for favourable interactions due to its smaller HOMO-LUMO energy gap. DFT analysis assessed stability, showing comparable values for the investigated compounds. Molecular docking reveals promising binding affinities of phytochemicals, particularly procyanidin dimer B2. Computational analysis and MD simulation revealed superior stability to reference compounds. While initial predictions indicate a favourable safety profile, further experimental validation is crucial to confirm these findings and their therapeutic potential.

Keywords: breast cancer; *Eugenia calycina*; procyanidin dimer B2; NUDT5; estrogen receptor alpha (ERα); phytochemicals; molecular docking; molecular dynamics; DFT.

1. Introduction

The overexpression of estrogen receptor alpha (ERα) in breast cancer is closely linked to poor clinical outcomes and resistance to therapeutic interventions. As a critical receptor in

the pathology of breast cancer, ERα presents a valuable target for therapeutic strategies aimed at inhibiting cancer cell growth and proliferation. By focusing on ERα, it is possible to develop treatments that more effectively control breast cancer progression, as it regulatesenes crucial for cell survival, differentiation, and proliferation [1–3]. Additionally, ERα modulates cytochrome-1B1 (CYP1B1), a protein that produces the metabolite 4-hydroxyestradiol, which increases reactive oxygen species and promotes neoplastic transformation in breast cancer cells [4]. Significantly, the expression level of ERα in breast cancer cells is elevated to 70%, in sharp contrast to the 7-17% observed in normal breast cells [5].

NUDT5, an ADP ribose pyrophosphatase, hydrolyzes ADPR, regulates its intracellular concentration, and maintains normal cellular physiological activities. Overexpression of NUDT5 is observed in breast cancer tissues and is linked to poorer overall survival in hormone receptor-positive breast cancer [6]. Inhibition of NUDT5 has reduced breast cancer cell growth *in vitro* and *in vivo*, highlighting its potential as a therapeutic target. NUDT5 influences ERα signaling in breast cancer cells by modulating ADP-ribose metabolism and interacting with hormone-signaling pathways [7]. Combining NUDT5 inhibition with targeting ERα could enhance anticancer therapy effectiveness, particularly in hormone receptor-positive breast cancers, where ERα is a key driver of tumorigenesis, and NUDT5 contributes to disease progression. By targeting both ERα and NUDT5, there is potential to further reduce cancer cell growth and proliferation, potentially improving treatment outcomes.

Several cancer drugs, including vinblastine, camptothecin, podophyllotoxin, and paclitaxel, are derived from botanical secondary metabolites or their semisynthetic derivatives and are used in the clinical treatment of various cancers. Natural products and their metabolites are currently regarded as valuable sources of active molecules, which can be used either as standalone treatments or in combination with existing drugs to enhance pharmacological effects and contribute to anticancer therapy [8]. Among such natural sources is the genus *Eugenia*, which is rich in various biological compounds. Given the vast number of phytochemicals present in natural sources like *E. calycina*, an *in silico* computational approach represents a critical first step. This strategy allows rapid, cost-effective screening and prioritization of the most promising lead compounds, focusing subsequent, resource-intensive *in vitro* and *in vivo* laboratory work on candidates with the highest predicted efficacy and safety.

The *Eugenia* genus has long been used in traditional medicine to treat a variety of ailments, including wounds, flu, fever, cough, gout, hypertension, digestive and liver disorders, rheumatism, tonsillitis, sore throat, hemorrhoids, and diarrhea. It also serves as a diuretic, repellent, domestic and agricultural insecticide, antidiarrheal, antihypertensive, and antirheumatic [9]. Recent developments in anticancer research involving *Eugenia* extracts have evaluated *Eugenia pyriformis'* potential, demonstrating its ability to inhibit cell migration, a key factor in the metastasis of cervical cancer cells [10]. Among the species whose molecular properties have not been extensively studied is *Eugenia calycina*. This species contains 153 phytochemicals from various chemical classes distributed throughout its parts [11]. A report from [11] further identified that every part of this plant is a rich source of bioactive compounds. The pulp is particularly notable for its phenolic compounds, while the seeds and leaves provide phenolic compounds with important biological activities for human health. While the genus *Eugenia* is known for its rich phytochemical profile, the specific molecular mechanisms of *Eugenia calycina* as an antitumor agent remain largely unexplored. To the best of our knowledge, this is the first *in silico* investigation to systematically screen *E. calycina* fruit

compounds for dual inhibitory potential against both Estrogen Receptor alpha (ERα) and NUDT5. Most studies focus on single-target inhibition, but by evaluating this dual-targeting mechanism, our work provides a novel computational framework for its potential synergistic anti-breast cancer effects, prioritizing specific compounds for future experimental validation.

2. Materials and Methods

2.1. Materials.

The primary materials used in this study include two macromolecular targets: Estrogen Receptor Alpha (ERα) with PDB ID 3ERT (resolution: 1.90 Å) and NUDT5 with PDB ID 5NWH (resolution: 2.60 Å), both retrieved from the Protein Data Bank (https://www.rcsb.org/). As ligands, various phytochemical compounds derived from *Eugenia calycina* were selected based on the study by Peixoto Araujo *et al*. (2020), with their 2D structures obtained from PubChem (https://pubchem.ncbi.nlm.nih.gov/). These ligands included Procyanidin Dimer B2 (PDB2), among others. The simulation environment employed water as a solvent (HOH residues) and an ionic concentration of 0.9% NaCl, simulating physiological conditions. Each enzyme was simulated at its respective physiological pH: pH 7.4 for ERα and pH 8.0 for NUDT5, with a temperature of 310 K (37 °C) to mimic the human biological environment [12].

2.2. Tools.

Several computational tools were employed to carry out structure preparation, molecular simulation, and toxicity prediction. YASARA Structure version 19.9.17 was used for protein and ligand preparation, and molecular docking using the dock_run.mcr macro, and molecular dynamics (MD) simulations using the md_run.mcr macro. Analysis parameters from MD simulations included RMSDbackbone, RMSF, and MM-PBSA binding free energy. To assess the electronic properties and reactivity of the ligands, Density Functional Theory (DFT) calculations were performed using Gaussian 09W with the B3LYP functional and 3-21G basis set, enabling the determination of HOMO, LUMO, and global chemical descriptors such as hardness, softness, electronegativity, and electrophilicity index. For toxicity prediction, Protox 3.0 (https://tox.charite.de/protox3/) was utilized, enabling *in silico* evaluation of hepatotoxicity, mutagenicity, carcinogenicity, p53 interaction, ERα interaction, and CYP1A2 modulation based on SMILES input data.

2.3. Preparation of enzymes and phytochemicals.

This study utilized two enzymes: estrogen alpha (PDB ID: 3ERT, resolution: 1.90 Å) and NUDT5 (PDB ID: 5NWH, resolution: 2.60 Å). Their three-dimensional (3D) structures were retrieved from the Protein Data Bank (https://www.rcsb.org/). Phytochemicals were identified from the work of Araujo *et al*. [11], and their 2D structures were obtained from PubChem (https://pubchem.ncbi.nlm.nih.gov/) (Figure 1). It is well-established that the initial 3D configuration of both the ligand and the enzyme significantly influences the quality of molecular docking simulations. Variations in decisions regarding protonation states and ligand tautomers for input into structure-based virtual screening (SBVS) protocols can lead to differing solutions. Yasara Structure (version 19.9.17) was employed to prepare the structures. Water molecules were removed for enzyme preparation, and hydrogen atoms were added, as

crystal structure resolution typically cannot predict hydrogen placement. In contrast, phytochemicals underwent energy minimization to optimize atomic positions within each ligand, resulting in structures with the lowest possible energy. Subsequently, these structures were protonated at a physiological pH of 7.4, followed by the generation of an ensemble of 3D conformations [13].

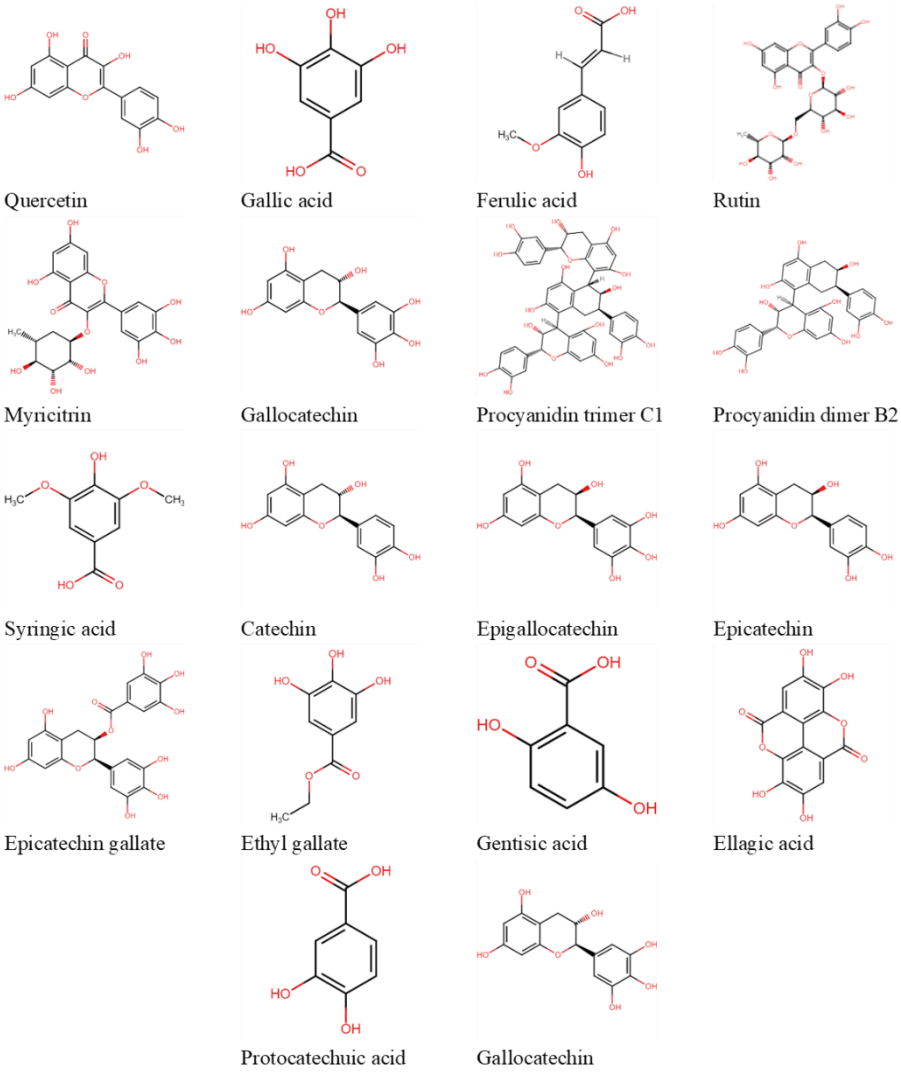

Figure 1. Two-dimensional phytochemical structures of *Eugenia calycina* fruit.

2.4. Prediction of toxicity.

All phytochemicals underwent *in silico* screening using Protox 3.0 (https://tox.charite.de/protox3/?site=contact). This web-based platform utilizes Simplified Molecular Input Line Entry System (SMILES) strings to predict potential toxicity. The screening parameters employed in this study included toxicity class, hepatotoxicity, neurotoxicity, carcinogenicity, mutagenicity, cytotoxicity, interaction with estrogen receptor alpha (ERα), binding to the tumor suppressor protein p53, and modulation of cytochrome P450 1A2 (CYP1A2) activity [14].

2.5. In silico binding analysis using molecular docking simulations.

To validate the accuracy and reliability of the docking protocol, a re-docking procedure was performed. The native ligands co-crystallized with each receptor (4-hydroxytamoxifen in 3ERT and the ligand in 5NWH) were extracted and re-docked into their respective binding

sites. The binding pose of the re-docked ligand was then superimposed on the original co-crystallized pose, and the Root Mean Square Deviation (RMSD) was calculated. An RMSD of less than 2.0 Å indicates successful validation, confirming that the protocol accurately reproduces the experimentally observed binding mode. Once the RMSD was confirmed to be less than 2.0 Å, the docking protocol predicted the binding scores and interactions between the enzymes and the phytochemicals. YASARA software analyzed the docked molecular complexes' comparative binding energies. YASARA Structure with the dock_run macro was utilized, performing 100 docking runs for each ligand. The binding energy score reported by YASARA can be interpreted as the sum of the intermolecular energy contribution from the lowest-scoring conformation and the intramolecular energy terms. A receptor grid with dimensions of 14.30 Å x 14.30 Å x 14.30 Å (spacing of 1 Å) was generated centered on the defined binding site residues of enzyme 3ERT. Similarly, a receptor grid with dimensions of 21.75 Å x 21.75 Å x 21.75 Å (spacing of 4 Å) was generated for enzyme 5NWH, encompassing its defined binding site residues. All docking results were subsequently analyzed and visualized [15].

2.6. Data analysis.

Ligand prioritization was performed using a scoring system that integrated toxicity and binding affinity. The final score for each ligand was calculated as the sum of several weighted components, detailed in Table 2. This included: a 'Toxicity Class Score' (Toxicity Class * 1000), binary toxicity flags for hepatotoxicity, neurotoxicity, etc. (+1000 for 'Inactive', -1000 for 'Active'), the LD50 value, and the binding energy scores for 3ERT and 5NWH (multiplied by -1 to make stronger, negative binding scores positive). This composite score allowed for a balanced prioritization of ligands with both favorable safety profiles and strong predicted binding interactions. Ligands with the highest final scores were then selected for further investigation using computationally more expensive methods, such as Density Functional Theory (DFT) calculations and Molecular Dynamics (MD) simulations. This scoring system facilitates the efficient identification of promising ligands with desirable toxicity profiles and binding solid interactions with the target molecule [14].

2.7. Molecular structure and reactivity analysis via density functional theory calculations.

This study employs density functional theory (DFT) calculations with complete geometry optimization for the selected molecular structures. Gaussian 09W software was utilized for optimization using the B3LYP method and the 3-21G basis set. The research subsequently calculates the HOMO and LUMO energy levels at the DFT level. These energy values serve as the foundation for the calculation of global chemical reactivity descriptors for the molecules, including hardness (η), chemical potential (μ), softness (S), electronegativity (χ), and electrophilicity index (ω). All calculations follow the methodology established by Irsal *et al*. [16].

2.8. Molecular dynamics (MD) simulation.

YASARA software was employed for all molecular dynamics (MD) simulations. Each simulation was run for 50 ns (nanoseconds) at a pH specific to the studied enzyme. Estrogen receptor alpha (ERα) (PDB ID: 3ERT) simulations were conducted at physiological pH 7.4 and a temperature of 37°C, mimicking typical cell culture conditions [17]. Conversely, simulations

for NUDT5 (PDB ID: 5NWH) were performed at physiological pH 8.0 and 37°C [18]. All simulations used a physiological ionic concentration of 0.9% NaCl (sodium chloride) as a mass fraction. The simulation temperature was set to 310 K, and the solvent was water (represented by HOH residues) with a density of 0.997 g/mL. To enhance computational efficiency, all simulation stages – preparation, minimization, equilibration, and production – were incorporated within a single script using the md_run.mcr macro. The AMBER 14 force field was employed for parameter calculations, and a non-bonded interaction cutoff of 20 Å was implemented. Due to the varying temperature simulations, the "#" symbol was removed from the "pressurectrl='Manometer1D, Pressure=1'" section within the macro to ensure proper pressure control. This study used three main analysis parameters: root-mean-square deviation of the backbone (RMSDbackbone), root-mean-square fluctuation (RMSF), and free-ergy calculations using the Molecular Mechanics Poisson-Boltzmann Surface Area (MM-PBSA) method [15].

3. Results and Discussion

3.1. Prediction of toxicity.

Analysis of the provided phytochemicals revealed a range of toxicity profiles and potential bioactivities (Table 1). Notably, most compounds exhibited no predicted hepatotoxicity, neurotoxicity, or estrogen receptor alpha. The carcinogenic potential was observed only in ellagic acid, protocatechuic acid, myricitrin, quercetin, and gallic acid. Meanwhile, all phytochemicals are inactive in cytotoxic activity. Interestingly, quercetin displayed the most diverse bioactivity profile, showing potential activity against carcinogenicity and mutagenicity, and was the only phytochemical predicted to activate the cytochrome CYP1A2 enzyme, which may be relevant for its metabolism and potential interactions with drugs. Hyperoside shows the potential to activate the tumor suppressor p53.

This research utilizes *in silico* techniques, a computational approach, to explore the antitumor potential of *Eugenia calycina* fruit. We focus on its ability to inhibit two key targets in breast cancer progression: nucleoside diphosphate 5 (NUDT5) enzyme and estrogen receptor alpha (ERα). *In silico* methods will investigate the interactions between *Eugenia calycina* fruit's compounds, NUDT enzymes, and ERα. This will provide valuable insights into the fruit's potential to disrupt these critical pathways in breast cancer. The research was initiated with the prediction of toxicity via Protox 3.0. The exploration of *Eugenia calycina* fruit phytochemicals revealed promising insights into their potential antitumor properties and safety profile. While the fruit's specific composition requires further investigation, the identified compounds offer valuable starting points for future research.

Encouragingly, most analyzed phytochemicals displayed no predicted hepatotoxicity, neurotoxicity, or binding affinity to ERα (Table 1). This suggests a potentially low risk of liver damage, neurological side effects, or hormonal imbalances associated with ERα activation, which are common concerns with some chemotherapeutic agents [19,20]. The predicted carcinogenicity of ellagic acid, protocatechuic acid, myricitrin, quercetin, and gallic acid warrants further investigation. While *in silico* predictions require experimental validation, these findings highlight the importance of future studies to determine their safety profile at relevant concentrations. It's crucial to assess if potential antitumor effects outweigh any carcinogenic risks. The diverse bioactivity profiles of the identified phytochemicals offer exciting possibilities. Quercetin stands out for its potential activity against carcinogenicity and

mutagenicity, as well as its unique ability to activate the CYP1A2 enzyme. This enzyme activation may be relevant to quercetin's metabolism and potential interactions with other drugs, warranting further exploration. Notably, all compounds were predicted to be inactive in cytotoxicity assays, suggesting a need for further *in vitro* and *in vivo* studies to confirm their antitumor effects. Hyperoside's predicted ability to activate the tumor suppressor p53 protein is another intriguing finding. p53 is critical in regulating cell growth and preventing uncontrolled proliferation, a hallmark of cancer. Activating p53 could potentially lead to tumor cell death or arrest of the cell cycle [21,22]—*t*he current study utilized *in silico* predictions, which provide valuable preliminary data. However, *in vitro* and *in vivo* experiments must validate these phytochemicals' predicted bioactivities and safety profiles. The favorable safety profile of most identified phytochemicals and their diverse bioactivities warrants further investigation.

3.2. Molecular docking.

To validate the docking protocol, the co-crystallized native ligands were extracted and re-docked into their respective binding sites. The protocol successfully reproduced the experimental binding poses, achieving a Root Mean Square Deviation (RMSD) of 1.81 Å for 3ERT (Figure 2A) and 1.87 Å for 5NWH (Figure 2B). As these values are below the 2.0 Å threshold for accuracy, the docking methodology was confirmed as valid for the subsequent virtual screening.

Several phytochemicals exhibited promising binding affinities in a virtual screening study targeting estrogen receptor alpha (PDB: 3ERT) and NUDT5 (PDB:5NWH) (Figure 3). For estrogen receptor alpha, 4-hydroxytamoxifen displayed the strongest binding energy (-10,017 kcal/mol), followed by procyanidin dimer B2 (-8.490 kcal/mol) and ellagic acid (-8.364 kcal/mol). Interestingly, several other compounds like catechin, epicatechin, and quercetin also demonstrated significant binding potential (binding energy > -8.000 kcal/mol). In comparison, NUDT5 showed a generally weaker binding profile. Procyanidin trimer C1 emerged as the top binder (-8.643 kcal/mol), while 7-[[5-(3,4-dichlorophenyl)-1,3,4-oxadiazol-2-yl]methyl]-1,3-dimethyl-8-piperazin-1-yl-purine-2,6-dione (TH5427) and procyanidin dimer B2 displayed moderate binding affinities (-8.288 kcal/mol and -8.185 kcal/mol, respectively). Notably, rutin, a flavonoid, exhibited substantial binding capacity to both targets (estrogen receptor alpha: -4.084 kcal/mol; NUDT5: -7.799 kcal/mol).

The *in silico* molecular docking simulations shed light on the potential interactions between *Eugenia calycina* fruit phytochemicals and two critical breast cancer targets: ERα and NUDT5 enzyme. These findings provide valuable insights into the fruit's potential mechanisms of action. The reference compounds utilized were 7-[[5-(3,4-dichlorophenyl)-1,3,4-oxadiazol-2-yl]methyl]-1,3-dimethyl-8-piperazin-1-yl-purine-2,6-dione or TH5427 (control for NUDT5, PDB: 5NWH) and tamoxifen (control for ERα, PDB: 3ERT). Tamoxifen (control drug in 3ERT) is a hormone therapy drug that blocks the effects of estrogen on breast cancer cells, making it particularly effective for hormone receptor-positive breast cancer. While anastrozole is commonly used for hormone receptor-positive breast cancer by inhibiting estrogen production, it was included as a control that does not naturally bind to these PDB targets.

Table 1. Toxicity prediction result from Protox III.

Phytochemicals	Toxicity Class	Hepatotoxicity	Neurotoxicity	Carcinogenicity	Mutagenicity	Cytotoxicity	Estrogen Receptor Alpha (ER)	Phosphoprotein (Tumor Supressor) p53	Cytochrome CYP1A2
Ellagic acid	4	Inactive	Inactive	Active	Inactive	Inactive	Inactive	Inactive	Inactive
Ferulic acid	4	Inactive	Inactive	Inactive	Inactive	Inactive	Inactive	Inactive	Inactive
Gallic acid	4	Inactive	Inactive	Active	Inactive	Inactive	Inactive	Inactive	Inactive
Gentisic acid	5	Inactive	Inactive	Inactive	Inactive	Inactive	Inactive	Inactive	Inactive
Protocatechuic acid	4	Inactive	Inactive	Active	Inactive	Inactive	Inactive	Inactive	Inactive
Ethyl gallate	6	Inactive	Inactive	Inactive	Inactive	Inactive	Inactive	Inactive	Inactive
Syringic acid	4	Inactive	Inactive	Inactive	Inactive	Inactive	Inactive	Inactive	Inactive
Catechin	6	Inactive	Inactive	Inactive	Inactive	Inactive	Inactive	Inactive	Inactive
Epicatechin gallate	4	Inactive	Inactive	Inactive	Inactive	Inactive	Inactive	Inactive	Inactive
Gallocatechin	6	Inactive	Inactive	Inactive	Inactive	Inactive	Inactive	Inactive	Inactive
Myricitrin	5	Inactive	Inactive	Active	Inactive	Inactive	Inactive	Inactive	Inactive
Epicatechin	6	Inactive	Inactive	Inactive	Inactive	Inactive	Inactive	Inactive	Inactive
Epigallocatechin	6	Inactive	Inactive	Inactive	Inactive	Inactive	Inactive	Inactive	Inactive
Procyanidin dimer B2	5	Inactive	Inactive	Inactive	Inactive	Inactive	Inactive	Inactive	Inactive
Procyanidin trimer C1	5	Inactive	Inactive	Inactive	Inactive	Inactive	Inactive	Inactive	Inactive
Quercetin	3	Inactive	Inactive	Active	Active	Inactive	Inactive	Inactive	Active
Hyperoside	5	Inactive	Inactive	Inactive	Inactive	Inactive	Inactive	Active	Inactive
Rutin	5	Inactive	Inactive	Inactive	Inactive	Inactive	Inactive	Inactive	Inactive

Table 2. Analysis of *in silico* screening.

Phytochemicals	TC score	HT score	NT score	CC score	MC score	CytC score	ER score	p53 score	CYP1A2 score	3ERT score	5NWH score	Total score	Average score
Ellagic acid	4000	1000	1000	-1000	1000	1000	1000	1000	1000	8364	7522	25886	2353.27
Ferulic acid	4000	1000	1000	1000	1000	1000	1000	1000	1000	6489	5991	24480	2225.45
Gallic acid	4000	1000	1000	-1000	1000	1000	1000	1000	1000	5701	5395	21096	1917.82
Gentisic acid	5000	1000	1000	1000	1000	1000	1000	1000	1000	5750	5225	23975	2179.55
Protocatechuic acid	4000	1000	1000	-1000	1000	1000	1000	1000	1000	5750	5225	20975	1906.82
Ethyl gallate	6000	1000	1000	1000	1000	1000	1000	1000	1000	6349	5717	26066	2369.64
Syringic acid	4000	1000	1000	1000	1000	1000	1000	1000	1000	5645	5406	23051	2095.55
Catechin	6000	1000	1000	1000	1000	1000	1000	1000	1000	8062	7008	29070	2642.73
Epicatechin gallate	4000	1000	1000	1000	1000	1000	1000	1000	1000	7453	7720	27173	2470.27
Gallocatechin	6000	1000	1000	1000	1000	1000	1000	1000	1000	7122	6915	28037	2548.82
Myricitrin	5000	1000	1000	-1000	1000	1000	1000	1000	1000	7171	7708	25879	2352.64
Epicatechin	6000	1000	1000	1000	1000	1000	1000	1000	1000	8062	7008	29070	2642.73
Epigallocatechin	6000	1000	1000	1000	1000	1000	1000	1000	1000	7122	6915	28037	2548.82
Procyanidin dimer B2	5000	1000	1000	1000	1000	1000	1000	1000	1000	8490	8185	29675	2697.73
Procyanidin trimer C1	5000	1000	1000	1000	1000	1000	1000	1000	1000	6418	8643	28061	2551.00
Quercetin	3000	1000	1000	-1000	-1000	1000	1000	1000	-1000	7762	6741	19503	1773.00
Hyperoside	5000	1000	1000	1000	1000	1000	1000	-1000	1000	7325	6621	24946	2267.82
Rutin	5000	1000	1000	1000	1000	1000	1000	1000	1000	4084	7799	24883	2262.09

Fwd: TC = toxicity class, HT = hepatotoxicity, NT = neurotoxicity, CC = carcinogenicity, MC = mutagenicity, CytC = cytotoxicity, ER = estrogen receptor alpha.

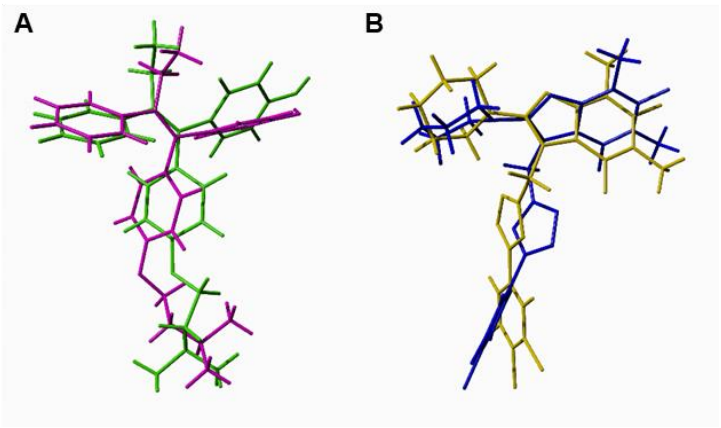

Figure 2. Validation of the docking protocol for **(A)** 3ERT; **(B)** 5NWH. (A) Superimposition of the co-crystallized 4-hydroxytamoxifen (shown in green) and the re-docked pose (shown in purple) within the 3ERT binding site. The calculated RMSD between poses is 1.81 Å. (B) Superimposition of the co-crystallized native ligand (yellow) and the re-docked pose (blue) within the 5NWH binding site, resulting in an RMSD of 1.87 Å.

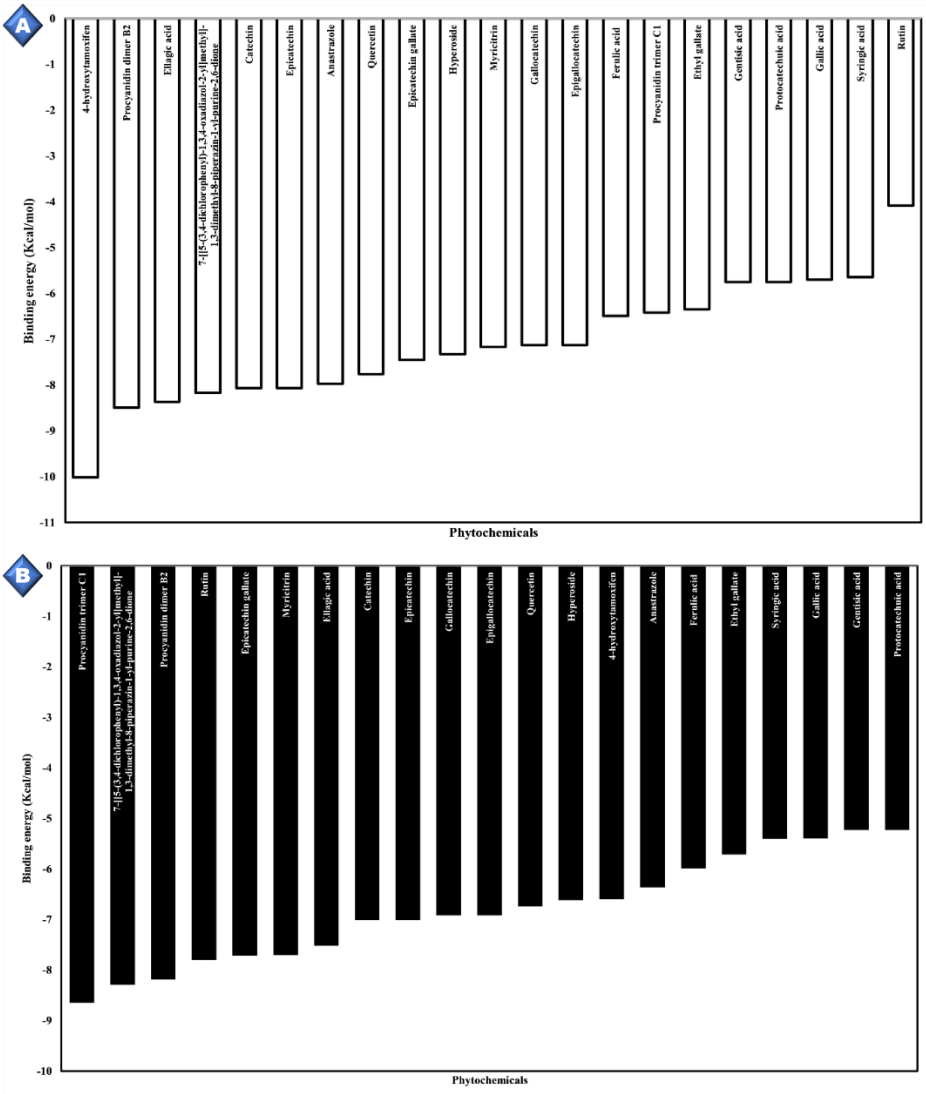

Figure 3. Molecular docking results when *Eugenia calycina* fruit attaches: **(a)** ERα; **(b)** NUDT5.

3.3. Data analysis.

Procyanidin dimer B2 emerged as the most favorable candidate with a high total score (29675) and average score (2967.73) in computational toxicity and virtual screening of various phytochemicals (Table 2). This favorable profile was attributed to its excellent performance in

multiple categories, including genotoxicity (TC score: 5000), hepatotoxicity (HT score: 1000), neurotoxicity (NT score: 1000), and cytotoxicity (CytC score: 1000). Procyanidin dimer B2 also demonstrated promising binding affinity to the estrogen receptor alpha (ER score: 8490). Conversely, quercetin displayed a concerning safety profile due to its negative scores in carcinogenicity (CC score: -1000) and mutagenicity (MC score: -1000), alongside a weak binding affinity to the estrogen receptor alpha (ER score: 7762). Interestingly, rutin exhibited substantial binding capacity to the estrogen receptor alpha (ER score: 4084) and NUDT5 (5NWH score: 7799) but possessed a moderate total score (24883) due to average performance in the genotoxicity and cytotoxicity categories. Overall, this *in silico* screening identified procyanidin dimer B2 as a promising phytochemical with favorable safety and potential bioactivity while highlighting potential concerns with quercetin.

This study highlights the critical value of *in silico* analysis for prioritizing promising phytochemicals from *Eugenia calycina* fruit. This approach offers a significant strategic advantage in the early stages of drug discovery. Traditionally, identifying drug candidates from natural sources relies on laborious, time-consuming, and expensive bioactivity-guided isolation and characterization techniques. *In silico* analysis, as implemented here, provides a powerful alternative. By integrating computational toxicity assessment and virtual screening, researchers can efficiently filter large chemical libraries to prioritize safe, potentially bioactive compounds such as PDB2 for focused experimental validation, therebyccelerating the development of novel therapeutic agents from natural sources [14]. PDB2 emerged as the most promising candidate due to its exceptional performance across multiple parameters. Its favorable *in silico* toxicity profile, as indicated by minimal concerns regarding genotoxicity, hepatotoxicity, neurotoxicity, and cytotoxicity, suggests a safe candidate for further investigation.

Additionally, its promising binding affinity towards ERα indicates potential antitumor activity. The analysis also effectively identified potential safety concerns with quercetin. Negative *in silico* predictions for carcinogenicity and mutagenicity warrant further investigation before considering it as a therapeutic candidate. This *in silico* filtering helps prioritize safer options early in development, saving time and resources. This study demonstrates the effectiveness of *in silico* analysis for prioritizing promising phytochemicals from *Eugenia calycina* fruit. This method offers a valuable tool for streamlining the initial stages of drug discovery. By integrating computational toxicity assessment and virtual screening, researchers can prioritize safe, potentially bioactive compounds such as PDB2 for further investigation, ultimately accelerating the development of novel therapeutic agents from natural sources.

3.4. Post-analysis of molecular docking.

Post-analysis identified procyanidin dimer B2 (PDB2) as the most promising phytochemical based on the data analysis. Subsequent investigations focused on its interactions with estrogen receptor alpha (ERα) and nucleoside diphosphate 5 (NUDT5). The dual-targeting mechanism of PDB2 offers a synergistic therapeutic effect by simultaneously inhibiting ERα and NUDT5 (Figure 4). These interactions appear to involve a variety of bonding forces, including van der Waals, hydrogen, π-cation, π-alkyl, attractive charge, π-sulfur, and salt bridges. Comparative analysis revealed that the reference compound, 4-hydroxytamoxifen, forms more interactions with ERα than procyanidin dimer B2 (Figure 5). Specifically, 4-hydroxytamoxifen (OHT) forms 25 bonds (including 1 hydrogen bond) compared to 18 bonds (including 2 hydrogen bonds) formed by PDB2 upon binding to ERα. Similarly, Figure 5

demonstrates that PDB2 interacts with NUDT5 through 24 bonds (including 6 hydrogen bonds), exceeding the interaction profile of the reference compound, 7-[[5-(3,4-dichlorophenyl)-1,3,4-oxadiazol-2-yl]methyl]-1,3-dimethyl-8-piperazin-1-yl-purine-2,6-dione (TH5427). TH5427 forms 22 bonds (including 4 hydrogen bonds) when bound to NUDT5 (Figure 6).

Post-docking analysis of PDB2 and 4-hydroxytamoxifen binding to ERα was conducted to elucidate the crucial residues involved in complex formation. Both ligands interacted with a network of amino acids, with some exhibiting ligand-specific roles. Several residues, including Met343, Thr347, Leu349, Ala350, Leu354, Trp383, and Leu384, were implicated in ligand binding for both PDB2 and 4-hydroxytamoxifen, corroborating their established importance in ERα interactions. PDB2 displayed a more prominent hydrogen bonding profile with ERα, forming interactions with Tyr526, Val534, Cys530 (π-sulfur), Lys529, Asp351 (carbon-hydrogen bond and π-anion), and Met528 (π-sulfur) (Figure 5A). These interactions likely contribute to its binding affinity. In contrast, 4-hydroxytamoxifen relied primarily on hydrophobic interactions with ERα, engaging with various residues such as Ala350 (π-alkyl), Arg394, Glu353, Leu346 (π-alkyl), Phe404, Leu387 (π-alkyl), Leu428 (π-alkyl), Ile424, Met388 (π-alkyl), Met421 (2 π-alkyl), and several other Leu residues (Figure 5B). Notably, it also formed a salt bridge with Trp383, potentially strengthening the complex. Both PDB2 (π-anion with Asp351) and 4-hydroxytamoxifen (interaction with Glu353) interacted with these residues, highlighting their contribution to complex stability and potentially influencing ligand potency.

Following *in silico* docking simulations of PDB2 and the reference compound TH5427 with NUDT5, a detailed analysis of the interacting residues was performed to elucidate their binding modes and identify key amino acids involved in ligand recognition. This post-docking analysis is essential for understanding the molecular basis of ligand-protein interactions. Both ligands interacted with Arg51, suggesting its potential role as an anchor residue for NUDT5 ligand binding. This finding is further supported by interactions with the Gly97 (carbon-hydrogen bond) formed by PDB2 and TH5427. The PDB2 exhibited a more diverse interaction profile with NUDT5, involving hydrogen bonds (Lys161, Asp100, Thr53, Arg51, Gln57, Ile99), π-interactions (Trp28, Arg54, Glu166), and hydrophobic contacts (Leu98, Arg84) (Figure 6A). These interactions likely contribute to its stronger binding affinity compared to TH5427. TH5427 relied more on hydrophobic interactions with NUDT5, engaging in π-alkyl interactions with Leu136, Val49, Val29, Met132, Ile341, Ala95, and Ala63 (Figure 6B). However, it also formed some hydrogen bonds (carbon-hydrogen bonds) with Gly97, Val62, Glu93, and Arg196. This post-docking analysis reinforces the significance of previously identified residues (Arg51, Gly97, Leu98) for NUDT5 ligand binding. It further reveals ligand-specific interaction patterns and identifies additional crucial residues (Met132, Cys139) for inhibitor recognition. This information can be leveraged in future studies for rational design and optimization of NUDT5 inhibitors with improved selectivity.

A docking pose was considered successful if the RMSD fell below the predefined threshold of 2.0 Å, which signifies high accuracy [23]. Gratifyingly, all receptors (ERα and NUDT5) yielded RMSD values below the 2.0 Å cutoff presented in Figure 9 (1.83 Å for ERα and 1.91 Å for NUDT5. This validates the accuracy of our docking methodology. The docking results revealed promising binding affinities of several phytochemicals with ERα (Fig. 3). Notably, 4-hydroxytamoxifen, a well-established ERα antagonist, was a positive control, exhibiting the strongest binding energy (-10.017 kcal/mol). Following closely behind 4-

hydroxytamoxifen were procyanidin dimer B2 (-8.490 kcal/mol) and ellagic acid (-8.364 kcal/mol). These findings suggest that these phytochemicals might possess ERα antagonistic properties similar to tamoxifen, potentially offering a natural alternative for ERα-positive breast cancer therapy. Furthermore, several other compounds, including catechin, epicatechin, and quercetin, displayed significant binding potential with energies exceeding -8.000 kcal/mol. These results warrant further investigation to explore their potential for ERα modulation and their impact on breast cancer cell proliferation.

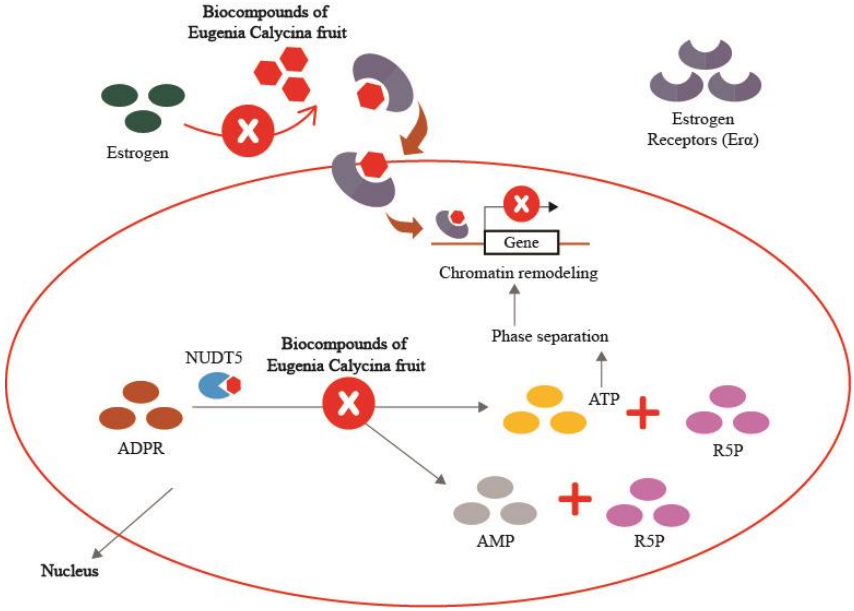

Figure 4. Potential inhibitory mechanism of action of *Eugenia calycina* fruit against ERα and NUDT5 in breast cancer.

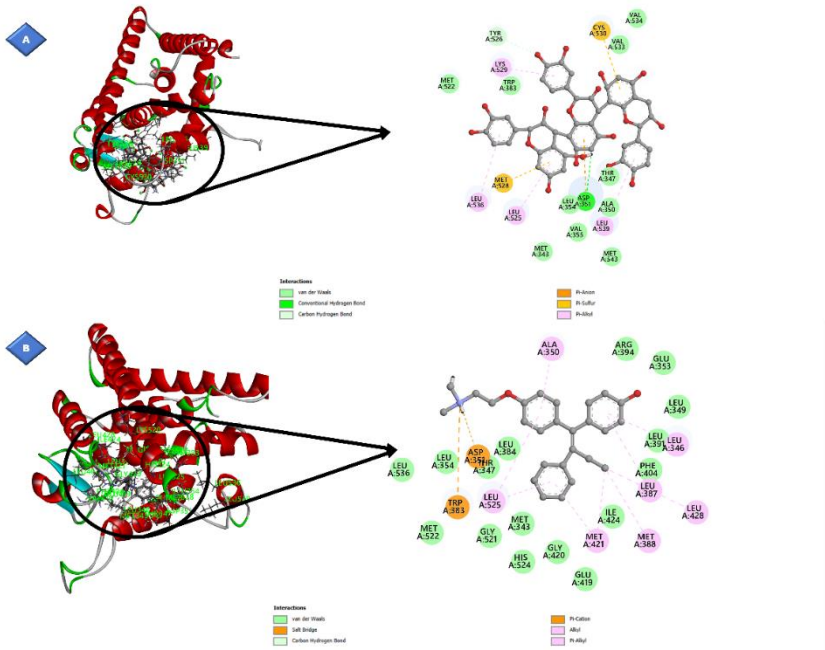

Figure 5. Interaction of *Eugenia calycina* fruit with ERα's pocket site: **(a)** Procyanidin dimer B2; **(b)** OHT.

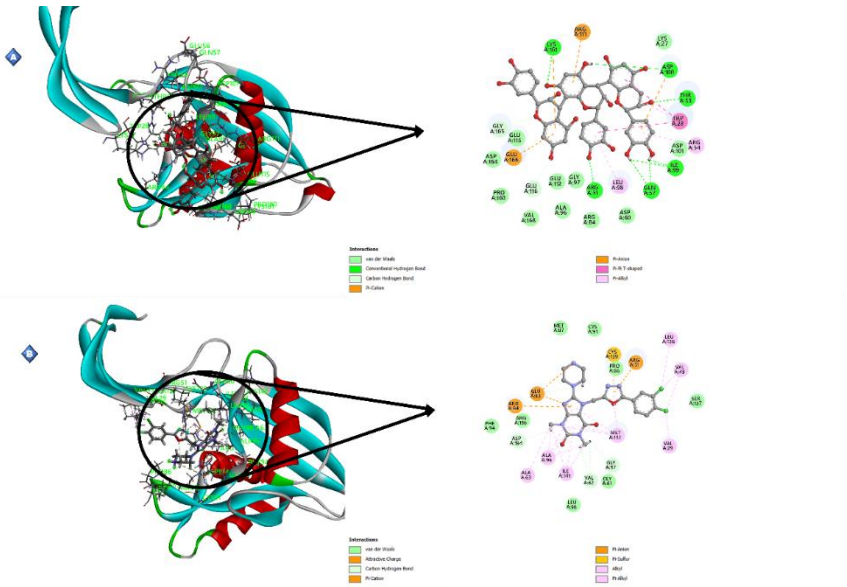

Figure 6. Interaction of *Eugenia calycina* fruit with NUDT5's pocket site: **(a)** Procyanidin dimer B2; **(b)** TH5427.

3.5. Density functional theory (DFT) calculations.

To provide a deeper rationale for the potential bioactivity, Density Functional Theory (DFT) calculations were performed. Understanding the electronic properties of a ligand, such as its HOMO-LUMO energy gap, is biologically crucial because it governs the molecule's ability to participate in electron-donating or -accepting interactions. These interactions are fundamental to forming stable covalent or non-covalent bonds with key amino acid residues within the active sites of target proteins, such as ERα and NUDT5.

Quantum chemical descriptors calculated using the DFT B3LYP method with the 3-21G basis set reveal interesting trends in the electronic properties of the investigated molecules [24]. The table summarizes the HOMO (highest occupied molecular orbital), LUMO (lowest unoccupied molecular orbital), and other quantum-chemical descriptors for three molecules: TH5427 (alpha and beta forms) and 4-hydroxytamoxifen (alpha and beta forms). The alpha form of TH5427 has the highest HOMO energy (-0.09676 eV), indicating its greatest propensity for electron donation. It also has the smallest energy gap (-0.06714 eV) compared to the other molecules, suggesting its potential for high reactivity. On the other hand, procyanidin dimer B2 produces the lowest HOMO energy (-0.20685 eV), signifying a lower tendency for electron donation. It also produces the highest energy gap (-0.19321 eV), potentially implying lower chemical reactivity. For the LUMO's value, 4-hydroxytamoxifen generates the highest number (0.00489 eV), indicating a greater ability to accept electrons. The beta form of TH5427 has the highest energy (-0.03368 eV), suggesting a moderate electron-accepting capability. Figure 7 depicts the HOMO, LUMO energies, and energy gap between HOMO and LUMO between the molecules. The color coding represents the orbitals' positive (green) and negative (red) phases [25]. This research has a unique case in that 1 molecule has 2 forms (alpha and beta). This happened to TH5427 and 4-hydroxytamoxifen (Figure 7).

Based on the data provided (Table 3), the quantum chemical descriptors of the listed phytochemicals offer insights into their potential reactivity. Ionization potential (I), ranging from 0.0809 eV (4-hydroxytamoxifen alpha) to 0.20685 eV (PDB2), reflects the ease of electron removal. Lower ionization potential indicates a molecule's propensity to lose an electron, making 4-hydroxytamoxifen alpha and TH5427 alpha easier to ionize. Electron

affinity (A), positive for all listed values (-0.00489 eV to 0.2834 eV), suggests a tendency to gain electrons. The beta form of TH5427 (0,03368 eV) and 4-hydroxytamoxifen (0.2834 eV) exhibit stronger electron affinity than PB2 (0.01364 eV). Chemical potential (μ), calculated as the average ionization potential and electron affinity, provides insight into a molecule's tendency to gain or lose electrons. The values range from -0.119995 eV (TH5427 beta) to -0.03801 eV (4-hydroxytamoxifen alpha). A negative chemical potential indicates a preference to gain electrons, while a more positive value suggests electron donation. Electronegativity (χ), half the sum of ionization potential and electron affinity, reflects a molecule's ability to attract electrons toward itself. The values range from 0.03801 eV (4-hydroxytamoxifen alpha) to 0.119995 eV (TH5427 beta), mirroring the trend observed in electronegativity. Hardness (η), the difference between ionization potential and electron affinity, reflects the resistance to electron deformation. Here, hardness values range from 0.03357 eV (TH5427 alpha) to 0.096605 eV (PDB2), indicating that PDB2 is the hardest (least susceptible to electron deformation). Softness (S), the reciprocal of hardness, shows an inverse relationship. The electrophilicity index (ω), calculated based on ionization potential and electron affinity, reflects the ability to accept electrons. The trend observed here aligns with the previously mentioned electrophilicity trend, with TH5427 beta exhibiting the strongest electrophilic character, stronger than PDB2 (0.08341 eV). However, PBD2's electrophilicity index is stronger than all forms of 4-hydroxytamoxifen.

This *in silico* study employed density functional theory (DFT) calculations with the B3LYP method and the 3-21G basis set to investigate various phytochemicals' electronic properties and potential reactivity. Analysis of the highest occupied molecular orbital (HOMO) and lowest unoccupied molecular orbital (LUMO) energies, along with other quantum-chemical descriptors, provided valuable insights into their potential biological activity [26]. This data can also inform protein-ligand interactions and the potential of these compounds as inhibitors. The HOMO-LUMO energy gap, the difference between HOMO and LUMO energy levels, reflects a molecule's stability. A larger gap indicates a harder, less reactive molecule, while a smaller one signifies a softer, more reactive molecule. For optimal bonding and ease of electronic transitions, a smaller energy gap is preferred [27]. Based on the calculated energy gaps (Table 3), PDB2 exhibited the highest propensity for bond formation and easier electronic transitions due to its smallest energy gap (-0.19321 eV) compared to the reference compounds, beta-TH5427 (-0.17263 eV) and beta-4-hydroxytamoxifen (-0.13890 eV).

The presence of alpha and beta forms for TH5427 and 4-hydroxytamoxifen introduces an interesting aspect to this study (Figure 7). This conformational polymorphism likely arises from multiple molecular orbitals with similar energies. Such phenomena are often observed in complex structures with extended conjugated systems or those containing diverse atoms and functional groups. Further investigation into the subtle variations in electronic properties between these forms could yield valuable insights for future research.

The calculated quantum chemical descriptors, including ionization potential (I), electron affinity (A), chemical potential (μ), electronegativity (χ), hardness (η), softness (S), and electrophilicity index (ω), offer valuable insights into the chemical reactivity of these molecules. The χ is related to the molecule's electron-donating properties and is the μ's negative in the Mulliken sense. The η and μ are defined as the second and first derivatives of the energy. Parr defined ω as a numerical value related to the stabilization of energy when the system acquires an electronic charge and serves as an indicator of the reactivity of a system towards

nucleophiles. The softness value is a property of molecules that measures the extent of chemical reactivity; it is the reciprocal of hardness [28].

Table 3. HOMO-LUMO energy values and other properties.

Phytochemicals		HOMO (eV)	LUMO (eV)	Energy gap (eV)	Ionization potential (I) (eV)	Electron affinity (A) (eV)	Chemical potentials (μ) (eV)	Electronegativity (χ) (eV)	Hardness (η) (eV)	Softness (S) (eV)	Electrophilicity index (ω) (eV)
7-[[5-(3,4-dichlorophenyl)-1,3,4-oxadiazol-2-yl]methyl]-1,3-dimethyl-8-piperazin-1-yl-purine-2,6-dione	alpha	-0.09676	-0.02962	-0.06714	0.09676	0.02962	-0.06319	0.06319	0.03357	14.89425	0.05947
	beta	-0.20631	-0.03368	-0.17263	0.20631	0.03368	-0.12000	0.12000	0.08632	5.79274	0.08341
4-hydroxytamoxifen	alpha	-0.0809	0.00489	-0.08579	0.08090	-0.00489	-0.03801	0.03801	0.04290	11.65637	0.01684
	beta	-0.1445	-0.2834	0.13890	0.14450	0.28340	-0.21395	0.21395	-0.06945	-7.19942	-0.32955
Procyanidin dimer B2		-0.20685	-0.01364	-0.19321	0.20685	0.01364	-0.11025	0.11025	0.09661	5.17572	0.06291

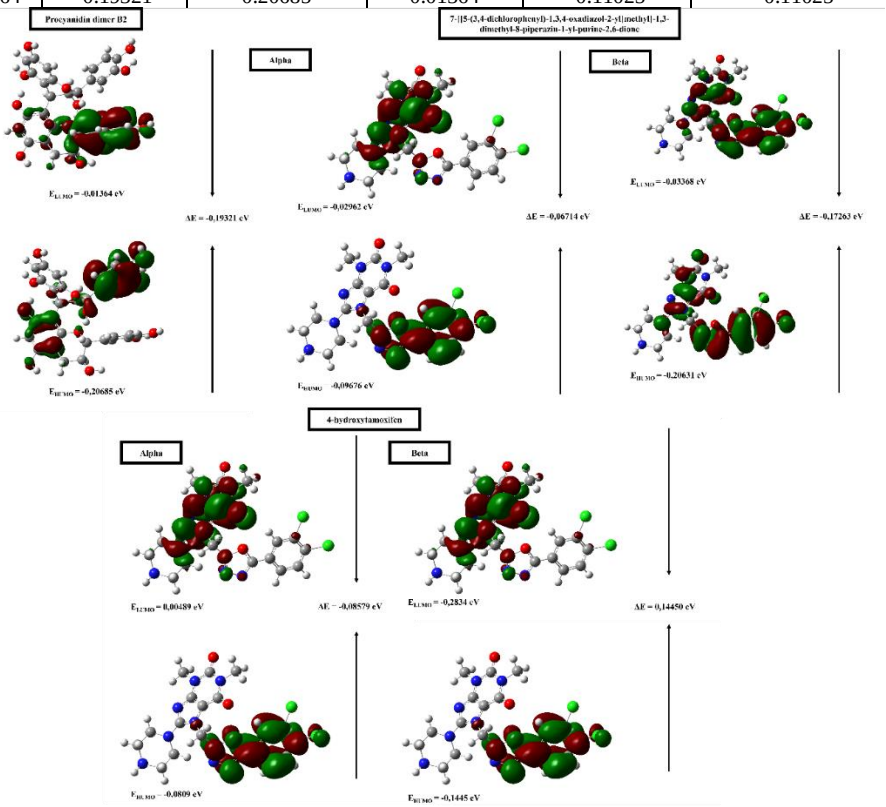

Figure 7. Visualization of the frontier molecular orbitals of rutin using the B3LYP/3-21G calculation method.

3.6. Molecular dynamics (MD) simulation.

To assess the stability and binding affinity of protein-ligand complexes, a 50-nanosecond (ns) molecular dynamics (MD) simulation was conducted. The study involved two target proteins, NUDT5 and estrogen receptor alpha (ERα) in complex with reference ligands, TH5427 and 4-hydroxytamoxifen, respectively, and a candidate phytochemical, procyanidin dimer B2 (PDB2). Structural stability and dynamic behavior were evaluated using root mean square deviation of backbone atoms ($RMSD_{backbone}$), root mean square fluctuation (RMSF), root mean square fluctuation (RMSF) of residues, and binding free energy calculations based on the molecular mechanics Poisson–Boltzmann surface area (MM-PBSA) method.

RMSD ($RMSD_{backbone}$) provides a quantitative measure of structural deviations over time, offering insight into the conformational stability of protein-ligand complexes [29]. As expected, all systems exhibited an initial increase in $RMSD_{backbone}$ due to equilibration, followed by stabilization (Fig. 8). The PDB2-NUDT5 complex demonstrated greater stability compared to the TH5427-NUDT5 reference system, with a lower average $RMSD_{backbone}$ value of 3.068 ± 0.72 Å versus 5.539 ± 1.16 Å. This suggests that PDB2 forms a more stable interaction with NUDT5, maintaining consistent relative positioning throughout the simulation. In the case of ERα, both the PDB2 and 4-hydroxytamoxifen complexes achieved equilibrium, though the PDB2-ERα complex exhibited a slightly higher average $RMSD_{backbone}$ (2.833 ± 0.47 Å) compared to 4-hydroxytamoxifen-ERα (2.118 ± 0.33 Å). Higher $RMSD_{backbone}$ values, as seen in the TH5427-NUDT5 and PDB2-ERα complexes, may indicate increased conformational flexibility or structural fluctuations, potentially suggesting a less rigid complex. In contrast, the lower $RMSD_{backbone}$ observed in the PDB2-NUDT5 and 4-hydroxytamoxifen-ERα complexes reflects enhanced structural stability.

The root mean square fluctuation (RMSF) provides a residue-level assessment of conformational flexibility, highlighting regions of structural rigidity or dynamic motion within protein-ligand complexes. Lower RMSF values indicate more rigid, stable regions, while higher values correspond to greater flexibility [30,31]. As shown in Figure 9, the PDB2-NUDT5 complex exhibited an average RMSF of 2.195 Å, indicating higher rigidity compared to the TH5427-NUDT5 complex (2.456 Å). Similarly, the 4-hydroxytamoxifen-ERα complex demonstrated a lower average RMSF (1.513 Å) than the PDB2-ERα complex (1.558 Å). These results suggest that PDB2 stabilizes the NUDT5 protein more effectively than the native ligand, whereas in the ERα system, the reference ligand provides slightly greater structural rigidity. Nevertheless, the differences in RMSF values for the ERα complexes are minimal and may not translate to biologically significant variations in overall stability.

The binding free energies of all complexes were estimated using the MM-PBSA approach implemented within the YASARA Structure suite. This method evaluates the energetic favorability of complex formation by incorporating molecular mechanics, polar solvation, and non-polar solvation contributions [32]. To obtain a more accurate estimation of binding affinity beyond docking scores, we utilized the Molecular Mechanics Poisson-Boltzmann Surface Area (MM-PBSA) method. This approach provides a quantitative measure of binding free energy, accounting for solvent effects and thermal fluctuations, thus simulating a realistic physiological environment. A highly negative binding free energy indicates a stable and favorable ligand-protein complex *in vivo*. As illustrated in Figure 10, PDB2 exhibited significantly more favorable binding free energies compared to the reference ligands. The PDB2-NUDT5 complex demonstrated a binding free energy of -286.193 ± 86.39 kJ/mol,

markedly lower than that of the TH5427-NUDT5 complex (-102.374 ± 100.09 kJ/mol). Likewise, PDB2 binding to ERα yielded a binding free energy of -365.015 ± 84.64 kJ/mol, outperforming the 4-hydroxytamoxifen-ERα complex (-17.584 ± 61.51 kJ/mol). The significantly more negative MM-PBSA binding free energy of PDB2 (-286.193 kJ/mol) with NUDT5 is not merely a numerical advantage; it suggests a highly stable, energetically favorable interaction that is mechanistically distinct from the reference. This pronounced stability, supported by the formation of six conventional hydrogen bonds (Figure 5A) with key residues such as Lys161 and Asp100, likely translates into a longer residence time at the active site. This could lead to sustained inhibition of NUDT5's enzymatic activity, offering a more durable therapeutic effect compared to the reference ligand.

The 50 ns simulation timeframe, although relatively short compared to longer MD studies, provides a balance between computational efficiency and detailed molecular insights. This duration is widely accepted for high-throughput screening of potential ligands and offers a reliable preliminary evaluation of binding stability and affinity [33,34].

Overall, the simulation results highlight procyanidin dimer B2 as a promising phytochemical with strong binding affinity and favorable interaction stability with both NUDT5 and ERα. The observed superior stability and binding energetics, particularly in the NUDT5 system, underscore the potential of PDB2 as a lead compound for further development. Nonetheless, future experimental studies are essential to validate these computational findings and elucidate the therapeutic applicability of PDB2.

While this study provides strong computational evidence for the potential of Procyanidin dimer B2 (PDB2) as a dual-target inhibitor, it is essential to acknowledge its limitations. The primary limitation is the *in silico* nature of the investigation. All findings, including binding affinities, stability, and toxicity profiles, are predictive and require rigorous experimental validation. The toxicity predictions, derived from Protox 3.0, offer a preliminary safety assessment but cannot replace *in vitro* cytotoxicity assays or *in vivo* toxicological studies. Furthermore, the 50 ns molecular dynamics simulations provide valuable initial insights into complex stability, but longer simulations could reveal additional conformational changes or long-term dynamic behaviors. The DFT calculations, while useful for understanding electronic properties, were performed with the 3-21G basis set; employing higher-level basis sets could yield more refined quantum chemical descriptors. Despite these limitations, the implications of this study are significant. It is the first to identify *Eugenia calycina* fruit as a source of potential dual inhibitors for both ERα and NUDT5, highlighting a promising multifaceted therapeutic strategy. The identification of PDB2 as a high-priority candidate validates the strategic utility of multi-step *in silico* screening for accelerating drug discovery from natural products, saving considerable time and resources compared to traditional methods.

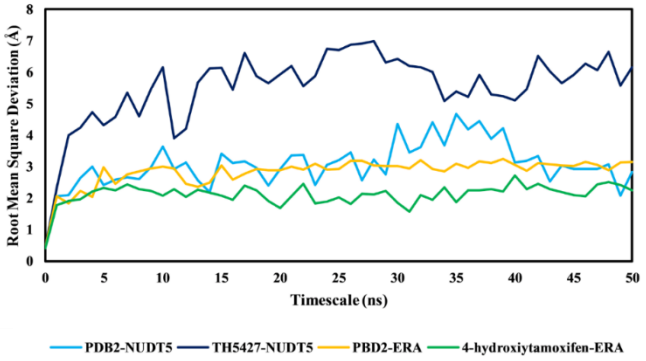

Figure 8. Root mean square deviation results along a 50 ns trajectory applied to NUDT5 and Erα.

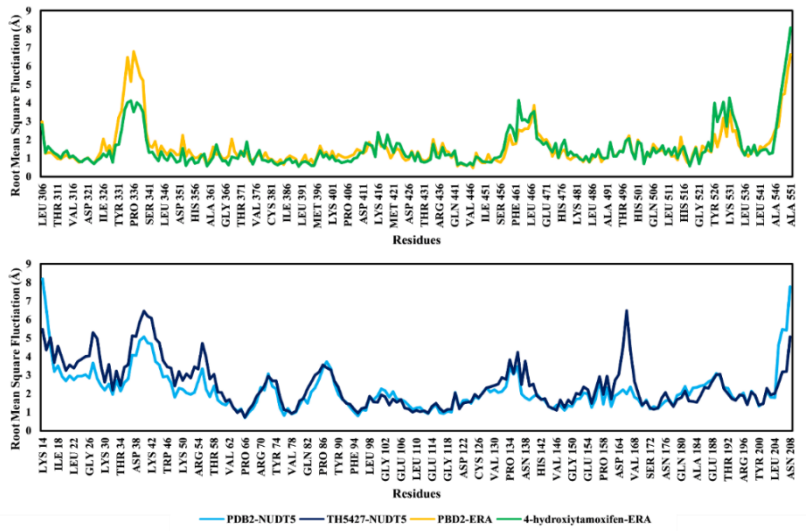

Figure 9. Root mean square fluctuation results of complexes over a trajectory of 50 ns.

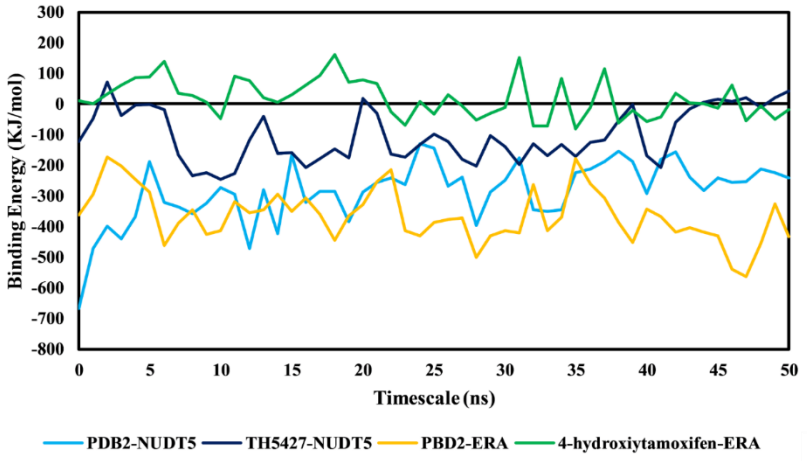

Figure 10. Binding energy results with MM-PBSA calculation over a trajectory of 50 ns.

4. Conclusions

Through a comprehensive *in silico* approach procyanidin dimer B2 (PDB2) was identified as a promising phytochemical candidate with a predicted favorable safety profile and potent binding affinity towards both ERα and NUDT5 through a comprehensive *in silico* approach, including toxicity prediction, molecular docking, and molecular dynamics simulations. The results indicate that PDB2 exhibits superior binding stability compared to reference compounds, as evidenced by lower $RMSD_{backbone}$ and RMSF values in molecular dynamics simulations. Furthermore, MM-PBSA calculations revealed significantly more negative binding free energies for PDB2 with both NUDT5 and ERα, suggesting stronger interactions. Quantum chemical calculations provided insights into the electronic properties of the compounds, revealing PDB2's potential for favourable interactions due to its smaller HOMO-LUMO energy gap. This research provides a strong foundation for further investigation into the anti-breast cancer potential of *E. calycina* fruit. Procyanidin dimer B2 emerges as a promising *in silico* lead compound, and these computational findings provide a strong rationale for advancing it into experimental validation. While this study provides strong computational evidence, it is essential to acknowledge its limitations. The findings are entirely *in silico* and predictive. The toxicity assessment, based on Protox 3.0, requires confirmation with *in vitro* cytotoxicity assays.

Furthermore, the 50 ns MD simulations provide initial stability insights but may not capture all long-term dynamic behaviors. Therefore, these *in silico* findings must be interpreted as a preliminary prioritization, and rigorous experimental validation is essential. Future work must focus on *in vitro* studies to confirm the biological activity of PDB2, such as cell viability assays using ER-positive breast cancer cell lines (e.g., MCF-7 and T-47D) and enzyme inhibition assays to quantify its IC50 values against ERα and NUDT5. Following successful *in vitro* validation, *in vivo* studies using rodent tumor xenograft models would be essential to assess the compound's efficacy, pharmacokinetics, and safety profile in a living organism. By targeting both ERα and NUDT5, PDB2 offers a potential, multifaceted approach, and this research provides the necessary justification for advancing it as a high-priority candidate for the development of effective, less toxic anticancer therapies.

Author Contributions

Conceptualization, R.A.P.I., F.C., and T.F.M.; methodology, F.C., T.F.M., and D.A.F.; software, R.A.P.I., A.T.N., and D.A.F.; validation, R.A.P.I., G.M.G., and S.H.; formal analysis, F.C. and T.F.M.; investigation, R.A.P.I., F.C., and T.F.M.; resources, R.A.P.I.; data curation, R.A.P.I., F.C., T.F.M., D.A.F., and G.M.G.; writing—original draft preparation, R.A.P.I., F.C., T.F.M., M.A.D., and D.A.F.; writing—review and editing, all authors; visualization, R.A.P.I., F.C., and T.F.M.; supervision, R.A.P.I.; project administration, R.A.P.I.; funding acquisition, R.A.P.I. All authors have read and agreed to the published version of the manuscript.

Institutional Review Board Statement

Not applicable.

Informed Consent Statement

Not applicable.

Data Availability Statement

Data supporting the findings of this study are available upon reasonable request from the corresponding author.

Funding

This research received no external funding.

Acknowledgments

Not applicable.

Conflicts of Interest

The authors declare no conflict of interest.

References

1. Nursyarah, A.T.; Safithri, M.; Andrianto, D. Red Betel Leaf Bioactive Compounds as ERα Receptor Inhibitors *In silico* and MCF-7 Cell Anticancer *In vitro*. *Hayati J. Biosci.* **2023**, *30*, 789-796, https://doi.org/10.4308/hjb.30.5.789-796.
2. Parikesit, A.A.; Ansori, A.N.M.; Kharisma, V.D. Computational Design of siRNA Targeting *Homo sapiens* HER2 Splice Variant mRNA: A Potential Strategy for Breast Cancer Intervention. *Biosaintifika: J. Biol. Biol. Educ.* **2024**, *16*, 384-393, https://doi.org/10.15294/biosaintifika.v16i3.3685.
3. Alifiansyah, M.R.T.; Herdiansyah, M.A.; Pratiwi, R.C.; Pramesti, R.P.; Hafsyah, N.W.; Rania, A.P.; Putra, J.E.R.P.; Cahyono, P.A.; Muhammad, S.K.; Murtadlo, A.A.A. QSAR of acyl alizarin red biocompound derivatives of *Rubia tinctorum* roots and its ADMET properties as anti-breast cancer candidates against MMP-9 protein receptor: *In silico* study. *Food Systems* **2024**, *7*, 312-320, https://doi.org/10.21323/2618-9771-2024-7-2-312-320.
4. Min, J.Y.; Lee, G.H.; Khanal, T.; Jin, S.W.; Lee, S.Y.; Kim, H.G.; Hyon, J.Y.; Chung, Y.H.; Ha, S.K.; Han, E.H.; Jeong, H.G. Upregulation of CYP1B1 by hypoxia is mediated by ERα activation in breast cancer cells. *Am. J. Cancer Res.* **2022**, *12*, 2798-2816.
5. Porras, L.; Ismail, H.; Mader, S. Positive Regulation of Estrogen Receptor Alpha in Breast Tumorigenesis. *Cells* **2021**, *10*, 2966, https://doi.org/10.3390/cells10112966.
6. Tong, X.-Y.; Quan, Y.; Zhang, H.-Y. NUDT5 as a novel drug target and prognostic biomarker for ER-positive breast cancer. *Drug Discov. Today* **2021**, *26*, 620-625, https://doi.org/10.1016/j.drudis.2020.11.031.
7. Wright, R.H.G.; Beato, M. Role of the NUDT Enzymes in Breast Cancer. *Int. J. Mol. Sci.* **2021**, *22*, 2267, https://doi.org/10.3390/ijms22052267.
8. Oprean, C.; Ivan, A.; Bojin, F.; Cristea, M.; Soica, C.; Drăghia, L.; Caunii, A.; Paunescu, V.; Tatu, C. Selective *in vitro* anti-melanoma activity of ursolic and oleanolic acids. *Toxicol. Mech. Methods* **2018**, *28*, 148-156, https://doi.org/10.1080/15376516.2017.1373881.
9. de Souza, A.M.; de Oliveira, C.F.; de Oliveira, V.B.; Betim, F.C.M.; Miguel, O.G.; Miguel, M.D. Traditional uses, Phytochemistry, and antimicrobial activities of *Eugenia* species–a review. *Planta Med.* **2018**, *84*, 1232-1248, https://doi.org/10.1055/a-0656-7262.
10. De Paula Alves, T.; Toledo Martins Pereira, M.; Sardou Charret, T.; César Thurler Júnior, J.; Freimann Wermelinger, G.; Regina Baptista, A.; Kaufmann Robbs, B.; Sawaya, A.C.H.F.; D'Ávila Bitencourt Pascoal, V.; Cristina Rheder Fagundes Pascoal, A. Evaluation of the Antiproliferative Potential of *Eugenia pyriformis* Leaves in Cervical Cancer Cells. *Chem. Biodivers.* **2022**, *19*, e202200114, https://doi.org/10.1002/cbdv.202200114.
11. Peixoto Araujo, N.M.; Arruda, H.S.; dos Santos, F.N.; de Morais, D.R.; Pereira, G.A.; Pastore, G.M. LC-MS/MS screening and identification of bioactive compounds in leaves, pulp and seed from *Eugenia calycina* Cambess. *Food Res. Int.* **2020**, *137*, 109556, https://doi.org/10.1016/j.foodres.2020.109556.
12. Abdulsalam, H.; Hix, M.A.; Philip, L.; Singh, K.; Walker, A.R.; Nguyen, H.M. From Docking and Molecular Dynamics to Experimental Discovery: Exploring the Hydrophobic Landscapes of Heparanase to Design Potent Inhibitors. *J. Chem. Inf. Model.* **2025**, *65*, 6899-6912, https://doi.org/10.1021/acs.jcim.5c00371.
13. Irsal, R.A.P.; Gholam, G.M.; Dwicesaria, M.A.; Chairunisa, F. Computational investigation of *Y. aloifolia* variegate as anti-Human Immunodeficiency Virus (HIV) targeting HIV-1 protease: A multiscale *in-silico* exploration. *Pharmacol. Res. - Mod. Chin. Med.* **2024**, *11*, 100451, https://doi.org/10.1016/j.prmcm.2024.100451.
14. Supandi; Yeni; Merdekawati, F. *In silico* study of pyrazolylaminoquinazoline toxicity by lazar, protox, and admet predictor. *J. Appl. Pharm. Sci.* **2018**, *8*, 119-129, https://doi.org/10.7324/JAPS.2018.8918.
15. Irsal, R.A.P.; Gholam, G.M.; Dwicesaria, M.A.; Mansyah, T.F.; Chairunisa, F. Computational exploration of palmitoyl-protein thioesterase 1 inhibition by *Juniperus phoenicea* L. for anti-dementia treatment. *J. Taibah Univ. Med. Sci.* **2024**, *19*, 1165-1180, https://doi.org/10.1016/j.jtumed.2024.12.005.
16. Irsal, R.A.P.; Gholam, G.M.; Firdaus, D.A.; Liwanda, N.; Chairunisa, F. Molecular docking and dynamics of Xylocarpus granatum as a potential Parkinson's drug targeting multiple enzymes. *Borneo J. Pharm.* **2024**, *7*, 161-171, https://doi.org/10.33084/bjop.v7i2.6810.
17. Jouffre, B.; Acramel, A.; Belnou, M.; Santolla, M.F.; Talia, M.; Lappano, R.; Nemati, F.; Decaudin, D.; Khemtemourian, L.; Liu, W.-Q.; Maggiolini, M.; Eschalier, A.; Mallet, C.; Jacquot, Y. Identification of a human estrogen receptor α tetrapeptidic fragment with dual antiproliferative and anti-nociceptive action. *Sci. Rep.* **2023**, *13*, 1326, https://doi.org/10.1038/s41598-023-28062-9.
18. García-Saura, A.G.; Zapata-Pérez, R.; Martínez-Moñino, A.B.; Hidalgo, J.F.; Morte, A.; Pérez-Gilabert, M.; Sánchez-Ferrer, Á. The first comprehensive phylogenetic and biochemical analysis of NADH diphosphatases

reveals that the enzyme from *Tuber melanosporum* is highly active towards NAD^+. *Sci. Rep.* **2019**, *9*, 16753, https://doi.org/10.1038/s41598-019-53138-w.

19. Banerjee, P.; Ulker, O.; Ozkan, I.; Ulker, O.C. The investigation of the toxicity of organophosphorus flame retardants (OPFRs) by using *in silico* toxicity prediction platform ProTox- 3.0. *Toxicol. Mech. Methods* **2025**, *35*, 32-42, https://doi.org/10.1080/15376516.2024.2382815.
20. Muslikh, F.A.; Samudra, R.R.; Ma'arif, B.; Ulhaq, Z.S.; Hardjono, S.; Agil, M. *In silico* molecular docking and ADMET analysis for drug development of phytoestrogens compound with its evaluation of neurodegenerative diseases. *Borneo J. Pharm.* **2022**, *5*, 357-366, https://doi.org/10.33084/bjop.v5i4.3801.
21. Marei, H.E.; Althani, A.; Afifi, N.; Hasan, A.; Caceci, T.; Pozzoli, G.; Morrione, A.; Giordano, A.; Cenciarelli, C. p53 signaling in cancer progression and therapy. *Cancer Cell Int.* **2021**, *21*, 703, https://doi.org/10.1186/s12935-021-02396-8.
22. Su, Y.; Sai, Y.; Zhou, L.; Liu, Z.; Du, P.; Wu, J.; Zhang, J. Current insights into the regulation of programmed cell death by TP53 mutation in cancer. *Front. Oncol.* **2022**, *12*, 1023427, https://doi.org/10.3389/fonc.2022.1023427.
23. Isawi, I.H.; Obeidat, R.M.; Alnabulsi, S.; Al Zoubi, R. Identification of Novel HPK1 Hit Inhibitors: From *In silico* Design to *In vitro* Validation. *Int. J. Mol. Sci.* **2025**, *26*, 4366, https://doi.org/10.3390/ijms26094366.
24. Miao, Z.; Li, Z.; Teng, X.; Wang, H.; Zhou, Y.; Qiu, Y.; Li, C.; Liu, C.; Tan, Y. Density Functional Theory Calculations and Infrared Spectral Analysis of Lignin. *Molecules* **2024**, *29*, 5683, https://doi.org/10.3390/molecules29235683.
25. Abedin, M.M.; Pal, T.K.; Uddin, M.N.; Alim, M.A.; Sheikh, M.C.; Paul, S. Synthesis, quantum chemical calculations, *in silico* and *in vitro* bioactivity of a sulfonamide-Schiff base derivative. *Heliyon* **2024**, *10*, e34556, https://doi.org/10.1016/j.heliyon.2024.e34556.
26. Irsal, R.A.P.; Gholam, G.M.; Dwicesaria, M.A.; Mansyah, T.F.; Chairunisa, F. Exploring the potential of *Scabiosa columbaria* in Alzheimer's disease treatment: An *in silico* approach. *J. Taibah Univ. Med. Sci.* **2024**, *19*, 947-960, https://doi.org/10.1016/j.jtumed.2024.09.003.
27. Sindhu, M.S.; Poonkothai, M.; Thirumalaisamy, R. Phenolic and terpene compounds from *Plectranthus amboinicus* (Lour.) Spreng. Act as promising hepatic anticancer agents screened through *in silico* and *in vitro* approaches. *S. Afr. J. Bot.* **2022**, *149*, 145–159, https://doi.org/10.1016/j.sajb.2022.06.001.
28. Rathod, S.; Shinde, S.; Choudhari, P.; Sarkate, A.; Chaudhari, S.; Shingan, A. Exploring binding potential of two new indole alkaloids from *Nauclea officinalis* against third and fourth generation EGFR: druglikeness, *in silico* ADMET, docking, DFT, molecular dynamics simulation, and MMGBSA study. *Nat. Prod. Res.* **2025**, *39*, 2970-2977, https://doi.org/10.1080/14786419.2023.2301678.
29. Biswas, S.; Mahmud, S.; Mita, M.A.; Afrose, S.; Hasan, M.R.; Sultana Shimu, M.S.; Saleh, M.A.; Mostafa-Hedeab, G.; Alqarni, M.; Obaidullah, A.J.; Batiha, G.E.-S. Molecular Docking and Dynamics Studies to Explore Effective Inhibitory Peptides Against the Spike Receptor Binding Domain of SARS-CoV-2. *Front. Mol. Biosci.* **2022**, *8*, 791642, https://doi.org/10.3389/fmolb.2021.791642.
30. Das, R.; Tamang, B.; Bhattarai, A.; Najar, I.N. Novel L-asparaginase from *Paucilactobacillus vaccinostercus*: Insights into anti-cancer potential using metagenomic, molecular docking and molecular dynamics simulation. *Microbe* **2025**, *7*, 100390, https://doi.org/10.1016/j.microb.2025.100390.
31. Costa, N.S.; Lima, L.R.; Cruz, J.N.; Santos, I.V.F.; Silva, R.C.; Maciel, A.A.; Barros, E.S.; Andrade, M.L.D.S.; Ramos, R.S.; Kimani, N.M.; Aragón-Muriel, A.; Álvarez-Caballero, J.M.; Campos, J.M.; Santos, C.B.R. Identification of Inhibitors with Potential Anti-Prostate Cancer Activity: A Chemoinformatics Approach. *Pharmaceuticals* **2025**, *18*, 888, https://doi.org/10.3390/ph18060888.
32. Jha, R.K.; Khan, R.J.; Amera, G.M.; Singh, E.; Pathak, A.; Jain, M.; Muthukumaran, J.; Singh, A.K. Identification of promising molecules against MurD ligase from *Acinetobacter baumannii*: insights from comparative protein modelling, virtual screening, molecular dynamics simulations and MM/PBSA analysis. *J. Mol. Model.* **2020**, *26*, 304, https://doi.org/10.1007/s00894-020-04557-4.
33. Afzal, M.A.F.; Browning, A.R.; Goldberg, A.; Halls, M.D.; Gavartin, J.L.; Morisato, T.; Hughes, T.F.; Giesen, D.J.; Goose, J.E. High-Throughput Molecular Dynamics Simulations and Validation of Thermophysical Properties of Polymers for Various Applications. *ACS Appl. Polym. Mater.* **2021**, *3*, 620-630, https://doi.org/10.1021/acsapm.0c00524.
34. Elfiky, A.A.; Mahran, H.A.; Ibrahim, I.M.; Ibrahim, M.N.; Elshemey, W.M. Molecular dynamics simulations and MM-GBSA reveal novel guanosine derivatives against SARS-CoV-2 RNA dependent RNA polymerase. *RSC Adv.* **2022**, *12*, 2741-2750, https://doi.org/10.1039/D1RA07447D.

Publisher's Note & Disclaimer